Progress In Electromagnetics Research B, Vol. 14, 263–283, 2009

TRANSMISSION LINE MODELING AND NUMERICAL SIMULASION FOR THE ANALYSIS AND OPTIMUM DESIGN OF METAMATERIAL MULTILAYER STRUCTURES

H. Oraizi and M. Afsahi

Department of Electrical Engineering
Iran University of Science and Technology
Narmak, Tehran 16844, Iran

Abstract—The transmission line transfer matrix method (TLTMM) is proposed for the analysis of planar multilayer metamaterial (MTM) structures, where a transmission line model is developed by the transfer matrix method. This novel method may consider any oblique incident plane wave at any angle of incidence, any linear polarization (TE or TM with respect to the incidence plane), circular and elliptical polarizations, any frequency range (microwave or optical frequencies), any number of layers, any combination of common materials (DPS) and MTMs (such as DNG, ENG, MNG), any layer thickness, consideration of any dispersion relations for ε and μ, etc. A unified formulation is presented for both TE and TM polarizations, which lead to the evaluation of the fields and powers inside the layers and half spaces. The objective of the paper is to analyze and design several diverse problems of multilayered structures by TLTMM and a matrix method. The results of computations by TLTMM are agreed with the literature where possible and with the matrix method.

1. INTRODUCTION

Metamaterials (MTMs) are such materials that at least one of their constants namely permittivity ($\varepsilon = \varepsilon' - j\varepsilon''$) or permeability ($\mu = \mu' - j\mu''$) is negative. Accordingly, common materials having positive permittivity ε and permeability μ are designated as double positive (DPS or right-handed). MTMs having only the real part of their ε negative are designated as epsilon-negative (ENG) and those MTMs

Corresponding author: H. Oraizi (h_oraizi@iust.ac.ir).

having only the real part of their permeability negative are designated as mu-negative (MNG). If both ε and μ have negative real parts, the MTM is called double negative (DNG or left-handed) [1]. The entropy conditions show that simultaneously negative ε and μ are physically impossible in a non-dispersive medium since they would violate the law of entropy [2]. Here we study the macroscopic behavior of MTMs, which are considered as homogeneous and isotropic dielectrics having the real parts of ε or μ or both negative.

Dielectric multilayer structures made up of common materials and structures have already been proposed in the literature and they have extensive applications in the microwave, millimetric waves (MMW) and optical frequency ranges. Several numerical and analytical methods have already been devised for the analysis of multilayer common material structures [3–8] multilayer MTM structures such as the propagation matrix method [9], the matrix method [1], and the iterative method [10].

In this paper, a formulation based on the combination of transmission line model and transfer matrix method namely Transmission Line Transfer Matrix Method (TLTMM) is proposed for the analysis of radio wave propagation in multilayered structures composed of common dielectrics and MTMs, which facilitates the analysis, design and optimization of the problems. Since the methods based on the equivalent transmission line model are simple, fast and accurate, so is TLTMM. It combines the treatment of TE and TM linear polarizations. Consequently, the analysis of the elliptically polarized waves (including the linear and circular polarizations) may be readily performed in a unified manner. The field solutions are obtained in all the regions of the stratified medium. First, the problem formulation is developed in MTM media and second several examples of the application of TLTMM are presented.

2. FORMULATION OF THE PROBLEM

Consider an isotropic and homogeneous MTM multilayer medium with boundary surfaces at $z = d_1, d_2, \ldots, d_N$ as shown in Fig. 1(a). It is analyzed by the TLTMM method and its results are validated by a matrix method and other simulated methods.

2.1. TLTMM Method

TLTMM develops an equivalent transmission line model as shown in Fig. 1(b) for multilayered planar structures under oblique incidence of an arbitrarily polarized plane wave. In this model, the transmission line

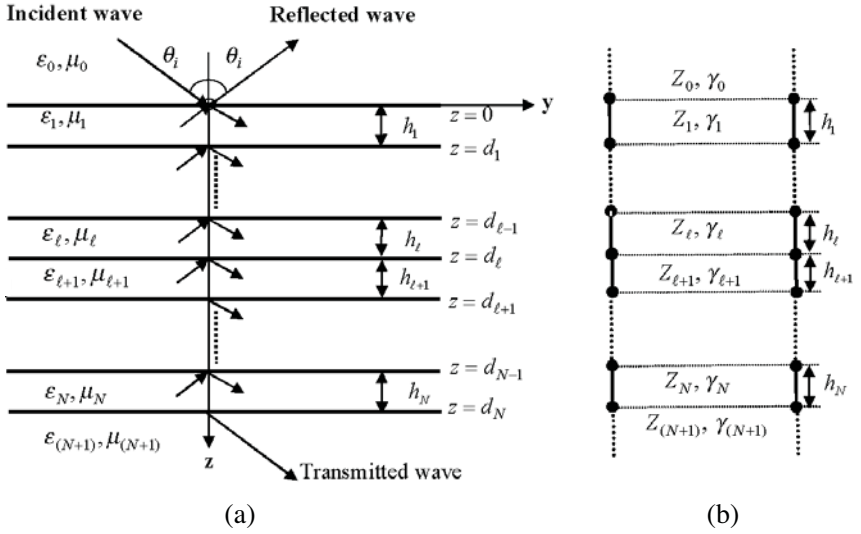

Figure 1. (a) A MTM multilayer structure. (b) The equivalent transmission line circuit model for an MTM multilayer structure.

section (ℓ) has characteristic impedance (Z_ℓ) and propagation constant ($\gamma_{\ell z}$) in the direction z normal to the structure, which depend on the angle of incidence, polarization and frequency of the incident plane wave. The characteristic impedanceof section ℓ of the transmission line model for TE and TM polarizations, is the wave impedance as the ratio of transverse components of electric and magnetic fields,

$$Z_\ell = \begin{cases} \sqrt{\mu_\ell/\varepsilon_\ell}\sec\theta_\ell & \text{for} \quad TE \\ \sqrt{\mu_\ell/\varepsilon_\ell}\cos\theta_\ell & \text{for} \quad TM \end{cases} \tag{1}$$

and the propagation constant of section ℓ of the transmission line, which is identical for both TE and TM polarizations, is

$$\gamma_{\ell z} = j\omega\sqrt{\mu_\ell \varepsilon_\ell}\cos\theta_\ell \tag{2}$$

where θ_ℓ is the incident angle in the ℓ'th layer according to the Snell's law

$$\gamma_\ell \sin\theta_\ell = \gamma_0 \sin\theta_0 \tag{3}$$

By TLTMM, the tangential components at the consecutive layers are related, which lead to two equations for two unknowns of reflection coefficient r and transmission coefficient t of the whole multilayer structure for TE, TM or elliptical polarizations [11]. r and t for the

TE and TM plane wave incidence are obtained from the following two dimensional matrix equation:

$$\begin{bmatrix} t \\ 0 \end{bmatrix} = [T]_{(N+1)0} \begin{bmatrix} 1 \\ r \end{bmatrix}, \tag{4a}$$

$$[T]_{(N+1)0} = [I]_{(N+1)N} \left([L]_N [I]_{N(N-1)} \right) \ \dots \ ([L]_1 [I]_{10}) \tag{4b}$$

where $[L]_\ell$ (for $\ell = 1, \dots, N$) is the wave amplitude transmission matrix in transmission line section ℓ

$$[L]_\ell = \begin{bmatrix} e^{-\gamma_{\ell z} h_\ell} & 0 \\ 0 & e^{\gamma_{\ell z} h_\ell} \end{bmatrix} \tag{5}$$

where h_ℓ is the length of equivalent TL of layer ℓ, which is equal to its thickness and $[I]_{(\ell+1)\ell}$ is the field amplitude transmission matrix of the ℓ'th section, which is different for TE and TM polarization

$$[I]^{TE}_{(\ell+1)\ell} = \frac{1}{1 - r^{TE}_{(\ell+1)\ell}} \begin{bmatrix} 1 & -r^{TE}_{(\ell+1)\ell} \\ -r^{TE}_{(\ell+1)\ell} & 1 \end{bmatrix} \tag{6}$$

$$[I]^{TM}_{(\ell+1)\ell} = \frac{1}{\left(1 + r^{TM}_{(\ell+1)\ell}\right) \frac{Z_{\ell+1}}{Z_\ell}} \begin{bmatrix} 1 & -r^{TM}_{(\ell+1)\ell} \\ -r^{TM}_{(\ell+1)\ell} & 1 \end{bmatrix} \tag{7}$$

where $r^{TE/TM}_{(\ell+1)\ell}$ and $t^{TE/TM}_{(\ell+1)\ell}$ are the Fresnel reflection and transmission coefficients between layers ℓ and $(\ell+1)$ for TE and TM polarization which are assumed to be the same as those between two half spaces [12].

By defining the variable

$$p^{TE/TM}_{(\ell+1)\ell} = \begin{cases} Z_{\ell+1}/Z_\ell & \text{for} \quad TE \\ Z_\ell/Z_{\ell+1} & \text{for} \quad TM \end{cases} \tag{8}$$

we may write matrices $[I]^{TE}_{(\ell+1)\ell}$ and $[I]^{TM}_{(\ell+1)\ell}$ in (6) and (7) in a unified form, where the characteristic impedances Z_ℓ are defined in (1).

$$[I]^{TE/TM}_{(\ell+1)\ell} = \frac{1}{2} \begin{bmatrix} 1 + p^{TE/TM}_{(\ell+1)\ell} & 1 - p^{TE/TM}_{(\ell+1)\ell} \\ 1 - p^{TE/TM}_{(\ell+1)\ell} & 1 + p^{TE/TM}_{(\ell+1)\ell} \end{bmatrix} \tag{9}$$

After computing the reflection coefficient r, the forward and backward traveling field amplitudes in the $\ell+1$'th layer, namely $C^{\pm}_{\ell+1}$ and $C^{\pm}_{\ell+1}$, may be determined by

$$\begin{bmatrix} C^+_{\ell+1} \\ C^-_{\ell+1} \end{bmatrix} = [I]_{(\ell+1)\ell} \left([L]_\ell [I]_{\ell(\ell-1)} \right) \ \dots \ ([L]_1 [I]_{10}) \begin{bmatrix} 1 \\ r \end{bmatrix} \tag{10}$$

We may now define reflectance $R = rr^*$, transmittance $T = tt^*$ and absorption $A = 1 - (R + T)$.

Table 1. The correct sign of propagation constant $\gamma_{\ell z}$ and characteristic impedance Z_ℓ of the transmission line model for lossless DPS, DNG, ENG and MNG media.

	ε	μ	Z_ℓ	$\gamma_{\ell z}$
DPS	$\varepsilon' > 0$	$\mu' > 0$	$\sqrt{\lvert \mu'/\varepsilon' \rvert} > 0$	$j\omega\sqrt{\lvert \mu'\varepsilon' \rvert} > 0$
DNG	$\varepsilon' < 0$	$\mu' < 0$	$\sqrt{\lvert \mu'/\varepsilon' \rvert} > 0$	$-j\omega\sqrt{\lvert \mu'\varepsilon' \rvert} < 0$
ENG	$\varepsilon' < 0$	$\mu' > 0$	$j\sqrt{\lvert \mu'/\varepsilon' \rvert} > 0$	$\omega\sqrt{\lvert \mu'\varepsilon' \rvert} > 0$
MNG	$\varepsilon' > 0$	$\mu' < 0$	$-j\sqrt{\lvert \mu'/\varepsilon' \rvert} < 0$	$\omega\sqrt{\lvert \mu'\varepsilon' \rvert} > 0$

For the extension of TLTMM for MTMs, if the time dependence is defined as $\exp(j\omega t)$, the imaginary parts of ε and μ should be negative to satisfy the law of conservation of energy. Furthermore, the correct sings of square roots in the expressions for Z_ℓ and $\gamma_{\ell z}$ of the equivalent transmission lines of MTMs should be selected. That is, their signs should be selected in such a way that in lossy MTMs the real parts of Z_ℓ are positive, because negative resistance indicates generation of energy in a medium and $\gamma_{\ell z}$ should be positive, because the wave should attenuate in the direction of propagation. Also in lossless MTMs only Z_ℓ of MNG and $\gamma_{\ell z}$ of DNG should be negative as shown in Table 1 [13].

Several points are noteworthy. First, it is possible to consider the ideal ground plane at the back of the multilayered MTM medium, which structure is applicable for the reduction of radar cross section (RCS). Second, the forward and backward propagating powers may be computed solely by the amplitude of forward and backward traveling waves for TE and TM polarization. Third, the reflection and transmission coefficients of each internal layer may be computed by Eq. (10). Fourth, in cases where one or more layers contain inhomogeneous materials, those layers may be subdivided into homogeneous sublayers with constant parameters, and the analysis may be carried out in a similar manner. Fifth, for the linear media, the reflectance due to the circularly polarized plane may be expressed in terms of those of TE and TM waves as

$$R^C = 0.5\left(R^{TE} + R^{TM}\right) \tag{11}$$

2.2. Matrix Method

The potential functions ψ in the half free space and multilayered regions may be written as (refer to Fig. 1):

$$\begin{aligned}
\psi_0^{TE/TM} &= e^{-\gamma_{0y}y}(e^{-\gamma_{0z}z} + r^{TE/TM}e^{\gamma_{0z}z}) \\
\psi_\ell^{TE/TM} &= e^{-\gamma_{\ell y}y}(C_\ell^+ e^{-\gamma_{\ell z}z} + C_\ell^- e^{\gamma_{\ell z}z}), \quad \ell = 1, \ldots, N \\
\psi_{N+1}^{TE/TM} &= e^{-\gamma_{\ell y}y}\left(t^{TE/TM}e^{-\gamma_{\ell(z+1)}z}\right)
\end{aligned} \tag{12}$$

where $r^{TE/TM}$ and $t^{TE/TM}$ are the reflection and transmission coefficients, $C_\ell^\pm$ are the normalized amplitudes of the forward and backward traveling waves in the ℓ'th layer, θ_ℓ is the angle of wave in the ℓ'th layer as in (3) and $\vec{\gamma}_\ell$ is the propagation vector in the ℓ'th layer as follows:

$$\vec{\gamma}_\ell = \hat{y}\gamma_{\ell y} + \hat{z}\gamma_{\ell z} = j\omega\sqrt{\mu_\ell\varepsilon_\ell}(\hat{y}\sin\theta_\ell + \hat{z}\cos\theta_\ell) \tag{13}$$

There are $2N + 2$ unknown amplitudes ($C_\ell^\pm$, $r^{TE/TM}$ and $t^{TE/TM}$) which may be obtained from the continuity of tangential electric and magnetic field components as in (14) at the $N + 1$ boundaries.

$$\begin{cases} E_x = -\partial\psi^{TE}/\partial y,\ H_y = 1/(j\omega\mu)\cdot\partial^2\psi^{TE}/\partial y\partial z & \text{for } TE \\ E_y = 1/(j\omega\varepsilon)\cdot\partial^2\psi^{TM}/\partial y\partial z,\ H_x = -\partial\psi^{TM}/\partial y & \text{for } TM \end{cases} \tag{14}$$

The set of equations for the boundary conditions may be written concisely as a matrix equation:

$$[A]\cdot[X] = [B] \tag{15}$$

where $[A]$, $[X]$ and $[B]$ are given in (16) and ξ is equal to μ_r and ε_r for the TE and TM waves, respectively. The numerical solution of (15) gives the unknown wave amplitudes and the coefficients r and t.

3. NUMERICAL EXAMPLES AND DISCUSSIONS

Several examples of oblique and normal incidence on different dispersive and non-dispersive MTM multilayered media are given below. Although MTMs are extremely dispersive [2], but they are assumed non-dispersive in several references [10, 14–16]. First, in this paper several non-dispersive examples (studied in these references) are treated by TLTMM to verify its effectiveness to analyze MTM media. Then, two examples with due consideration of dispersion phenomena are designed and optimized by the method of least squares

and combination of conjugate gradient (CG) and genetic algorithm (GA) to show new applications of MTMs.

The computer simulation of the proposed TLTMM may be described as follows: The inputs to the computer program are, type of polarization (TE or TM), angle of incidence (θ_i), operating

$$
\begin{aligned}
&[X] = \begin{bmatrix} r & C_1^+ & C_1^- & \dots & C_\ell^+ & C_\ell^- & \dots & C_N^+ & C_N^- & t \end{bmatrix}^T,\\
&[B] = \begin{bmatrix} -1 & -\gamma_{0z} & 0 & \dots & 0 & 0 & \dots & 0 & 0 & 0 \end{bmatrix}^T,\\
&A_{11} = 1, \quad A_{12} = -1, \quad A_{13} = -1,\\
&A_{21} = -\gamma_{0z}, \quad A_{22} = -\gamma_{1z}/\xi_1, \quad A_{23} = \gamma_{1z}/\xi_1,\\
&A_{2\ell+1,2\ell} = e^{-\gamma_{\ell z} d_\ell}, \quad A_{2\ell+1,2\ell+1} = e^{\gamma_{\ell z} d_\ell},\\
&A_{2\ell+1,2\ell+2} = -e^{-\gamma_{(\ell+1)z} d_\ell}, \quad A_{2\ell+1,2\ell+3} = -e^{\gamma_{(\ell+1)z} d_\ell},\\
&A_{2\ell+2,2\ell} = (\gamma_{\ell z}/\xi_\ell) e^{-\gamma_{\ell z} d_\ell}, \quad A_{2\ell+2,2\ell+1} = -(\gamma_{\ell z}/\xi_\ell) e^{\gamma_{\ell z} d_\ell},\\
&A_{2\ell+2,2\ell+2} = -(\gamma_{(\ell+1)z}/\xi_{\ell+1}) e^{-\gamma_{(\ell+1)z} d_\ell},\\
&A_{2\ell+2,2\ell+3} = (\gamma_{(\ell+1)z}/\xi_{\ell+1}) e^{\gamma_{(\ell+1)z} d_\ell},\\
&\ell = 1, 2, \dots, N-1\\
&A_{2N+1,2N} = e^{-\gamma_{Nz} d_N}, \quad A_{2N+1,2N+1} = e^{\gamma_{Nz} d_N},\\
&A_{2N+1,2N+2} = -e^{-\gamma_{(N+1)z} d_N},\\
&A_{2N+2,2N} = (\gamma_{Nz}/\xi_N) e^{-\gamma_{Nz} d_N}, \quad A_{2N+2,2N+1} = -(\gamma_{Nz}/\xi_N) e^{\gamma_{Nz} d_N},\\
&A_{2N+2,2N+2} = -(\gamma_{(N+1)z}/\xi_{(N+1)}) e^{-\gamma_{(N+1)z} d_N},\\
&\text{other } A_{ij} = 0, \quad i, j = 1, 2, \dots, 2N+2
\end{aligned}
\tag{16}
$$

frequency (f) and bandwidth, number of layers (N), thicknesses of layers (h_ℓ), constants of the layer materials ($\varepsilon_\ell, \mu_\ell$), constitutive parameters of the dispersion relations, etc. Then the transmission matrices $[L]_{(\ell+1)}$ from Eq. (5), parameters $p^{TE/TM}$ from Eq. (8) and the discontinuity transfer matrices $[I]_{(\ell+1)\ell}^{TE/TM}$ from Eq. (9) and then the overall transfer matrix $[T]_{(N+1)0}$ by Eq. (4b) are computed. Eventually the reflection and transmission coefficients (r, t) are computed by Eq. (4a) and then the values of R, T and A are calculated. The field and power variations may then be plotted against frequency, angle of incidence and position in the layers.

3.1. Single Frequency (Non-dispersive Metamaterials)

Three examples of non-dispersive media are analyzed by TLTMM to show its capabilities for the calculation of overall reflectance from 40 layer structures at normal incidence, the normalized H_x field and Poynting's vector inside and outside the layers for TM polarization of incident plane wave, and overall transmittance due to the evanescent wave in multilayer MTM media.

3.1.1. Examples 1. Distributed Bragg Reflection (DBR)

In this example, the reflection from the MTM multilayer structure is calculated by TLTMM and compared with the literature [14]. The distributed Bragg reflection (DBR) is made up of several pairs of layers. Each pair is composed of two layers with different permittivities. DBR exhibits high reflection in a frequency bandwidth called the Bragg regime. It has applications in waveguides, such as optical fibers [17–20]. DBR may be fabricated by common dielectric materials and by MTMs. However, DBR may be made of MTMs in wavelength regions, where it is impossible to fabricate them by solely common dielectrics. Fig. 2 shows the reflectance of a multilayer structure composed of 40 layers (DNG-DPS)^{20} as DBR. The layer pairs are taken as DNG-DPS with constants $\varepsilon_{DNG} = 4(-1 - j0.001)$, $\mu_{DNG} = 1.02(-1 - j0.001)$ and $\varepsilon_{DPS} = 1$, $\mu_{DPS} = 1$. The DNG medium may be considered a little lossy.

The thickness of a layer pair is equal to p and that of the DNG layer is equal to qp with $0 < q < 1$. Fig. 2 shows reflectance against

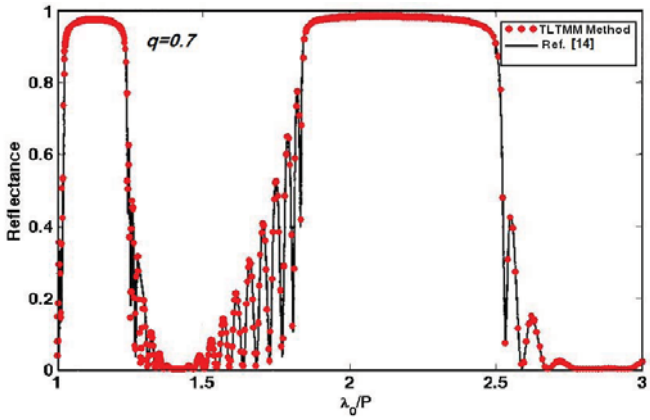

Figure 2. Reflectance of a 40 layer $(DNG - DPS)^{20}$ high reflection structure for normal plane wave incidence with wavelength λ_0.

wavelength for the value of $q = 0.7$. The results of the proposed TLTMM agree with those of [14].

3.1.2. Example 2. Anti-reflection Coating

It is possible to design double layer structures using MTMs in order to act as a anti-reflection surface for any angle of incidence. Realization of such a design is not possible by common dielectric materials. A pair of DNG-DPS layers with equal thicknesses and opposite signs for permittivity and permeability ($\varepsilon_{DNG} = -\varepsilon_{DPS}$, $\mu_{DNG} = -\mu_{DPS}$) placed between two half-spaces [21] and a pair of ENG-MNG layers with the selection of constants according to ($\varepsilon_{MNG} = -\varepsilon_{ENG}$, $\mu_{MNG} = -\mu_{ENG}$) placed between two half-spaces [1] produce an anti-reflection coating for any frequency and angle of incidence.

For the case of $d_{DPS}/\lambda_{DPS} = d_{DNG}/\lambda_{DNG} = 0.2$, $\varepsilon_{DPS} = 3.5\varepsilon_0$, $\mu_{DPS} = 2.5\mu_0$, $\varepsilon_{DNG} = -3.5\varepsilon_0$, $\mu_{DNG} = -2.5\mu_0$ and TM polarization of the indicated wave at the incidence angle $\theta_i = 45^\circ$ and arbitrary frequency f_0, the variation of H_x field and Poynting's vector in the z-direction (S_z) are plotted against position by TLTMM in Fig. 3. The normalized H_x field and Poynting's vector (relative to the incident wave) is drawn inside and outside the layers. The H_x field components in front of the structure ($z = 0$) and at its back ($z = h_1 + h_2$) are identical and also it is seen that the real parts of the normalized Poynting's vector is constant and is equal to unity across the layers, which is due to the complete tunneling of the incident wave and the reflection coefficient becoming zero. Fig. 4 shows the distribution of the real part of the Poynting's vector inside and outside the lossless DPS-DNG for the TM plane wave at the incident angle 45°, indicated in the title of Fig. 3. Here we see the complete flow of power through the slabs.

3.1.3. The Effect of Losses on the Image Quality of Nonperfect Lenses

A DNG layer in air makes a perfect lens [16, 21]. The waves emanating from an object hit a DNG layer, and produce transmitted waves of amplitude 1 and phase 0, which will then combine to create a complete image of the object. Since the DNG layer is inherently lossy, this is not realizable due to the principle of causality [23, 24].

The propagation vector in different layers is considered as $\vec{\gamma}_\ell = \gamma_{\ell x}\hat{x} + \gamma_{\ell z}\hat{z}$, where $\gamma_{\ell i} = \alpha_{\ell i} + j\beta_{\ell i}$ for $i = x, z$ and $\alpha_{\ell i}$ and $\beta_{\ell i}$ are the attenuation constant and phase constant in the directions $i = x, z$, respectively. The DNG media may be considered lossy, but the DPS media are assumed lossless with $\alpha_{\ell i} = 0$ and $k_x^2 + k_z^2 = \omega^2\mu_{DPS}\varepsilon_{DPS}$. If $|k_x| > \omega\sqrt{\mu_{DPS}\varepsilon_{DPS}}$, the wave traveling in the z

direction is evanescent. The evanescent waves in perfect lenses are actually amplifying, as opposed to the case in common lenses. For this reason, they are effective in the improvement of image quality [24].

Figure 5 depicts the concept of creation of an image by a multilayer structure and the perfect lens conditions ($\mu_{DNG} = -\mu_{DPS}$, $\varepsilon_{DNG} = -\varepsilon_{DPS}$, $h_\ell = h$, $\ell = 1, \ldots, N$). The image of object in the first layer (S) may be perfectly reproduced in the last layer (S'). The distance of object from the first boundary should be less than the thickness h, which is taken equal to $0.5h$ for simplicity. Therefore, the image S' is also at a distance of $0.5h$ from the last boundary. The number of layers (N) is odd. Any deviation of ε_{DNG} and μ_{DNG} from the perfect lens conditions adversely affect the image quality. This effect is expressed

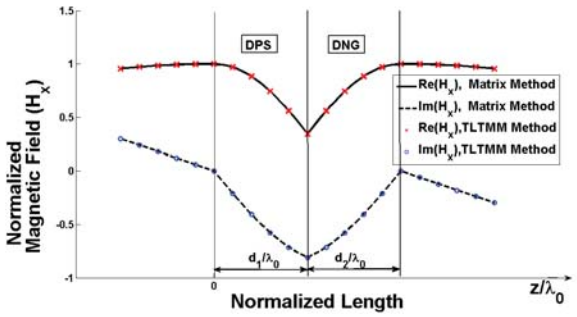

(a)

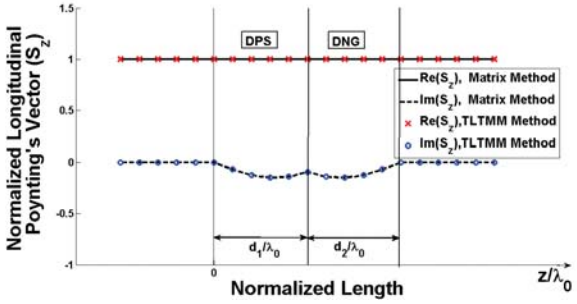

(b)

Figure 3. Variation of the field component H_x and Poynting's vector in z-direction (S_z) for TM polarization, angle of incidence 45° and frequency f_0. (a) Normalized H_x; (b) Real and Imaginary parts of normalized Poynting's vector.

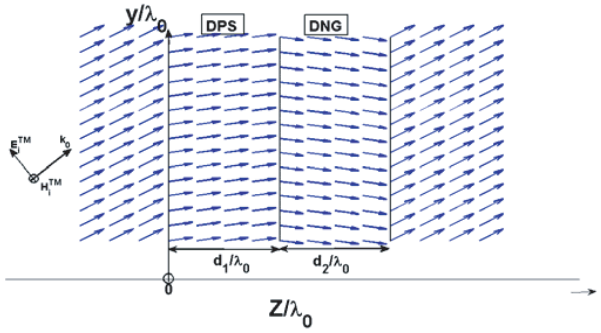

Figure 4. Distribution of the real part of the Poynting's vector inside and outside the lossless DPS-DNG for the TM plane wave at the incident angle 45°, specified in Fig. 3.

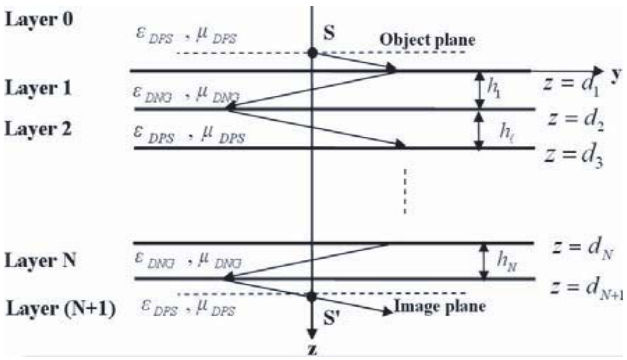

Figure 5. A periodic multilayer structure consisting of DNG and DPS layers, which is a perfect lens in the lossless case.

by a factor called recovery degree [16, 24]

$$q = |q|\, e^{j\phi_q} = \frac{A^+_{N+1} e^{-0.5\gamma_{(N+1)z}h}}{A^+_0 e^{0.5\gamma_{0z}h}} \tag{17}$$

where A^+_0 is the amplitude of the incident plane wave at the surface of the first layer, and A^+_{N+1} is that at the surface of the last layer. The perfect lens condition is evidently $q = 1$.

For minimizing the effect of dielectric losses due to ε and μ on the image quality, a DNG layer may be divided into several sublayers, which are placed in between the DPS layers. If the total thickness of layers of this structure is large enough, the value of $q = 1$ and consequently the excellent image quality is achieved [24].

Consider an evanescent plane wave impinging on a DNG layer along the z-direction. In Fig. 6, the recovery degree and phase shift are drawn versus k_y/k_0 and are compared with the DNG-DPS multilayer structure. This comparison is made subject to the similarity of DNG layers. The specifications are: $\varepsilon_{DNG} = -1 - j0.1$, $\mu_{DNG} = -1 - j0.001$, $\varepsilon_{DPS} = \mu_{DPS} = 1$, $k_0 h = 1$, 0.5, $\frac{1}{3}$ for $N = 1$, 3, 5, respectively.

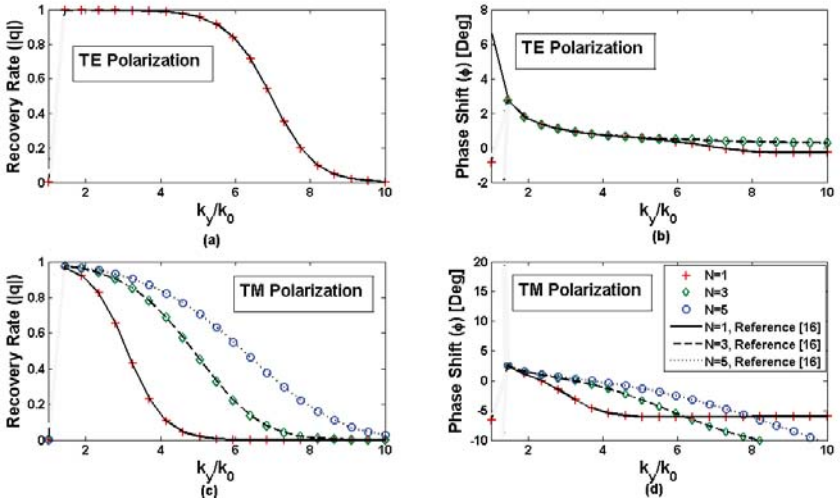

Figure 6. The recovery rate and phase shift of evanescent waves as a function of k_y for three different layer numbers when the total thickness of the DNG is invariable.

In Fig. 6, it is seen that the recovery degree for TE and TM waves increases with the increase of number of layers. Practically, with high enough number of layers, and large values of k_y, the recovery degree and phase shift are 1 and 0, respectively, particularly for TE waves. Furthermore, the phase shifts of TE and TM waves decrease with the increase of number of layers.

3.2. Multi Frequency (Dispersive Metamaterials)

Example 4 is presented for the validation of TLTMM method in dispersive media and examples 5 and 6 show the capabilities of TLTMM for the design of multilayer MTM structures for specific purposes.

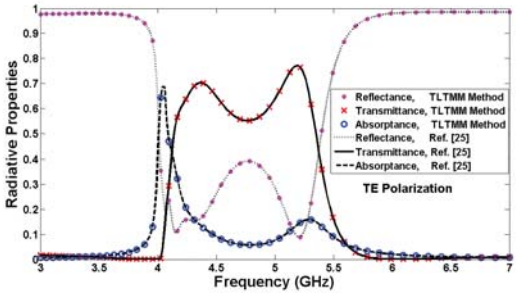

Figure 7. Radiative properties of DPS-DNG bilayer structure.

3.2.1. Example 4. Propagation Characteristics of Dispersive Metamaterials

In this example, the propagation characteristics in terms of power reflection, power transmission and power absorption of a DPS-DNG bilayer structure (including dispersion properties of DNG) are obtained. The parameters (ε_r, μ_r) of the media on the two sides of the bilayer are (2.25, 1), those of the DPS layer are (1, 1) and those of the DNG layer are according to Resonance and Drude's dispersion relations in Eqs. (18) and (19), respectively, with magnetic resonant frequency $f_{m0} = 4\,\text{GHz}$, electric plasma frequency $f_{ep} = 10\,\text{GHz}$, electric and magnetic damping factors $\Gamma_e = \Gamma_m = 30\,\text{MHz}$ and relative factor $F = 0.56$. The thickness of each layer is 8 mm, the incident wave is TE polarized, and the angle of incidence is 45°. The reflectance (R), transmittance (T) and absorption (A) are shown in Fig. 7. Power absorption occurs only in the DNG layer. Power transmittance has the highest value in the frequency range 4–6 GHz, where the real part of the refraction index of DNG layer is negative. Absorption curve has a maximum value near the resonance frequency 4 GHz. The results by TLTMM completely coincide with those of reference [25].

$$\mu_r = 1 - Ff^2/(f^2 - f_{m0}^2 - j\Gamma_m f) \tag{18}$$

$$\varepsilon_r = 1 - f_{ep}^2/(f^2 - j\Gamma_e f) \tag{19}$$

3.2.2. Example 5. Radar Absorbing Metamaterials

Absorbing materials have various applications such as stealth and shielding of high reflection surfaces. However, the fabrication of lossy magnetic materials having desirable dispersion relations at microwave frequencies is difficult and increases the weight of coatings Fabrication of wide band and wide angle RAMs being thinner and having less

weight will be possible by MTMs which may be an improvement over the available technologies [26]. Since the multilayer structures are infinite in the transverse directions, and the plane surfaces are assumed smooth, specular reflection occurs and scattering is ignored. Consequently, RCS is assumed proportional to reflectance. The even layers are composed of lossy DNG-MTMs with the Drude's and Lorentz dispersion relations in Eqs. (19) and (20), respectively, where f_{m0} is the magnetic resonant frequency, f_{mp} is the magnetic plasma frequency, and Γ_m is the magnetic damping factor [27, 28], and the odd layers are made of common lossy materials having the dispersion relation according to Eq. (21).

$$\mu_r = 1 - (f_{mp}^2 - f_{m0}^2)/(f^2 - f_{m0}^2 - j\Gamma_m f) \tag{20}$$

$$\varepsilon_c = \varepsilon' - j(\varepsilon'' + \sigma/\omega) \tag{21}$$

An error function is constructed in terms of reflectance by the method of least squares (MLS) in Eq. (22), where $t = 1, \ldots, 10$ indicates ten incident angles in the range of 0° to 80° and $f = 1, \ldots, 10$ indicates ten frequencies from 1 to 12 GHz and w_{tf} is a weighting function. The minimization of error function is achieved by the combination of GA and CG methods, which provides the fastest convergence towards the global minimum point of the error function.

$$Error = \sum_{t=1}^{10} \sum_{f=1}^{10} w_{tf} |R_{fb} + 20|^2 \tag{22}$$

The frequency response of a designed eight layer DPS-DNG RAM under the oblique incidence of a TE polarized plane wave is shown in Fig. 8. it is observed that for more than one frequency decade from 1 to 12 GHz and for wide range of angles from 0 to 75°, the reflectance is low. The parameters of the layers are given in Table 2.

3.2.3. Example 6. Dual Band Reflectors

Applications of wireless LAN and Wi-Fi frequency bands are rapidly expanding. They are used only indoors and they should not be transmitted to outdoors. Therefore, shielding of buildings should be implemented. However, stealth wallpaper can reflect the specific frequencies (wireless LAN and Wi-Fi) and transmit other frequencies (TV broadcasting, mobile services, etc) for the protection of indoor information. Fabrication of stealth wallpaper with MTM is a new application. For example, a dual band reflector with three-layers of MNG-MTM is designed for the obstruction of data transmission at 12

Table 2. Specification of an eight DPS-DNG pair RAM where the odd layers are composed of common lossy materials with $\mu_r = 1$ and the even layers are composed of split ring resonators and metallic thin wires.

Layer No.	Thickness (mm)	Dispersion Relation	Dispersion Parameters
1	10	21	$\varepsilon_r = 1.1293,\ \ \sigma = 14.9936$
2	4.8	19, 20	$f_{ep} = 1\,\text{GHz},$ $\Gamma_m = 28.7334\,\text{GHz}$ $f_{mp} = 8.6081\,\text{GHz},$ $f_{m0} = 7.0909\,\text{GHz},$ $\Gamma_m = 6.4500\,\text{GHz}$
3	4.5	21	$\varepsilon_r = 1.3920,\ \ \sigma = 14.9984$
4	9.6	19, 20	$f_{ep} = 1\,\text{GHz},$ $\Gamma_m = 28.7334\,GHz$ $f_{mp} = 5.8525\,\text{GHz},$ $f_{m0} = 3.5940\,\text{GHz},$ $\Gamma_m = 5.4400\,\text{GHz}$
5	9.9	21	$\varepsilon_r = 1.4034,\ \ \sigma = 14.9986$
6	1.4	19, 20	$f_{ep} = 1\,\text{GHz},$ $\Gamma_m = 28.7334\,\text{GHz}$ $f_{mp} = 19.6504\,\text{GHz},$ $f_{m0} = 4.6807\,\text{GHz},$ $\Gamma_m = 8.7073\,\text{GHz}$
7	9.2	21	$\varepsilon_r = 8.1963,\quad \sigma = 14.9992$
8	8.3	19, 20	$f_{ep} = 1\,\text{GHz},$ $\Gamma_m = 28.7334\,\text{GHz}$ $f_{mp} = 11.2008\,\text{GHz},$ $f_{m0} = 5.6229\,\text{GHz},$ $\Gamma_m = 6.8129\,\text{GHz}$

and 13 GHz for circularly polarized wave. The layers are composed of lossy MNG-MTMs with the dispersion relation in Eq. (20). An error function is constructed according to Eq. (23). Occurrence of transmittance is indicated by $b = 1, 2$ for frequencies 12 and 13 GHz and no transmittance is indicated by $b = 3, 4, 5$ for frequencies below 12 GHz and above 13 GHz and between 12 and 13 GHz. Also $f = 1, \ldots, 10$ indicates ten frequencies in each band, and $t = 1, \ldots, 10$

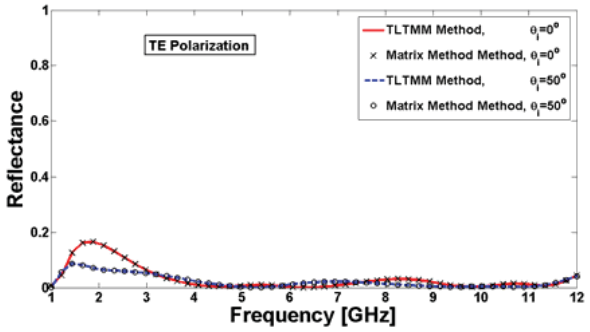
TE Polarization
TLTMM Method, θi=0°
Matrix Method Method, θi=0°
TLTMM Method, θi=50°
Matrix Method Method, θi=50°
Reflectance
Frequency [GHz]

(a)

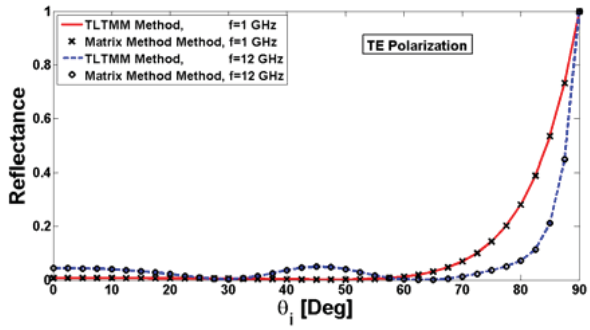
TLTMM Method, f=1 GHz
Matrix Method Method, f=1 GHz
TLTMM Method, f=12 GHz
Matrix Method Method, f=12 GHz
TE Polarization
Reflectance
θi [Deg]

(b)

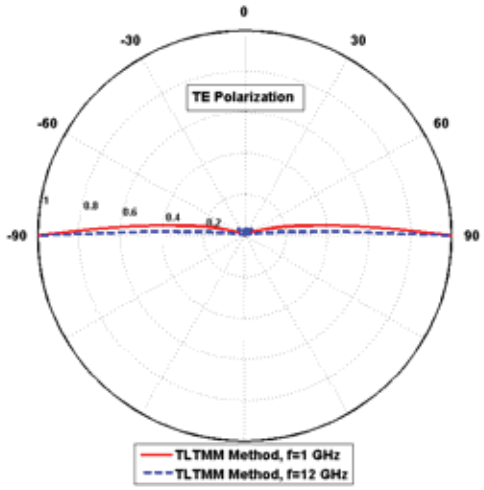
TE Polarization
TLTMM Method, f=1 GHz
TLTMM Method, f=12 GHz

(c)

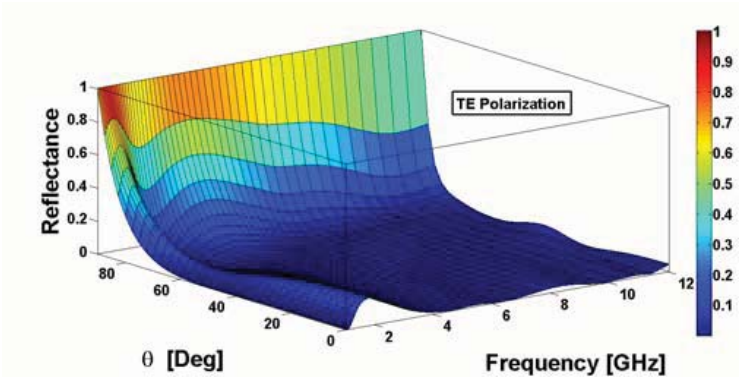

(d)

Figure 8. The reflectance of an eight DPS-DNG pair RAM coating composed of lossy common material and DNG-MTM under the TE polarized plane wave, at incident angle of 30°. (a) The reflectance versus frequency; (b) The reflectance versus incident angle; (c) The reflectance versus incident angle in polar plot, (d) 3-D reflectance manifold versus frequency and incident angle.

indicates ten incident angles from 0° to 60°. The minimization of error function is achieved by the combination of MLS, GA and CG.

$$Error = \sum_{t=1}^{10} \sum_{f=1}^{10} \left(\sum_{b=1}^{2} w_{tfb} |T_{fb} + 15|^2 + \sum_{b=3}^{5} w_{tfb} |T_{fb}|^2 \right) \tag{23}$$

Figure 9 shows the transmittance-frequency characteristic of a designed six layer MNG-MTM dual band reflector under the oblique incidence of a circular polarized plane wave and Table 3 shows its designed parameters.

TLTMM has some common features with TMM, but is based on the transmission line formulation. It therefore benefits from some physical interpretations and approach on the other hand; TLTMM provides a unified formulation for both TE and TM polarizations. The results from the TLTMM and TMM formulations are quite similar. Examples 1, 3 and 4 in references [4, 16] and [25] are solved by TMM and are solved by TLTMM in our paper for comparison.

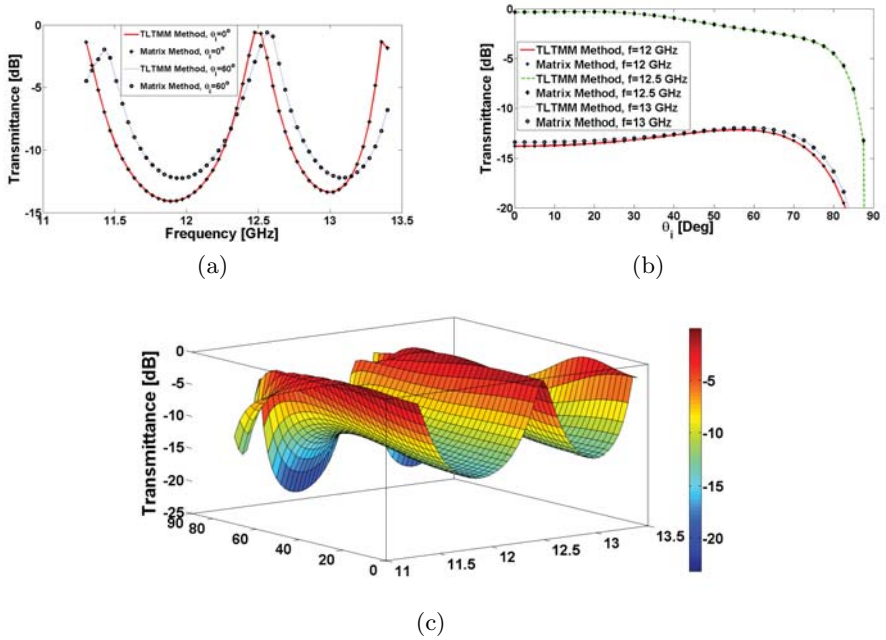

(a) (b)

(c)

Figure 9. The transmittance-frequency dependence of a dual reflector MNG-MTM under circular polarization. (a) The transmittance versus frequency; (b) The transmittance versus incident angle; (c) 3-D transmittance manifold versus frequency and incident angle.

Table 3. Specifications of six-layers of MNG-MTM as a dual band reflector, composed of split ring resonators with $\varepsilon_r = 1$.

Layer No.	Thickness (mm)	f_{mp} (GHz)	f_{m0} (GHz)	Γ_m (MHz)
1	4.7	841.6854	381.1716	1
2	1.4	886.7427	50.0068	1
3	1.7	915.3140	340.2613	1
4	1.8	900.4392	216.7181	1
5	1.6	871.9699	32.0342	1
6	3.5	878.5522	369.1462	0.8246

4. CONCLUSIONS

A method based on the Transmission Line Transfer Matrix Method (TLTMM) is implemented for the analysis of MTM multilayer structures. The frequency responses of reflected and transmitted waves of such multilayer structures are accurately determined by TLTMM, which exhibit dependence on frequency, angle of incidence, polarization of the incident wave,physical parameters of the stratified media, and dispersion relations of materials. The formulation of the combined TE and TM polarizations, leads to the generalized treatment of elliptically polarized waves (including linear and circular wave polarizations).

The field and power distributions inside and outside layers may be computed. The TLTMM may also be applied to MTM multilayer structures which are inhomogeneous in the variable normal to the layer surfaces.

Several examples were treated by the proposed TLTMM, such as anti-reflection coating, high reflection coating, distributed Bragg reflector (DBR), photon tunneling in MTMs, and the effect of losses on the image quality of nonperfect lenses. The results of computations by TLTMM agree very well with those available in the literature.

ACKNOWLEDGMENT

This research was in part supported by Iran Telecommunication Research Center under contract number 500/1911 dated 2007/5/8.

REFERENCES

1. Alù, A. and N. Engheta, "Pairing an epsilon-negative slab with a mu-negative slab: Resonance, tunneling and transparency," *IEEE Trans. Antennas Propagat.*, Vol. 51, No. 10, 2558–2571, 2003.
2. Veselago, V., "The electrodynamics of substances with simultaneously negative values of ε and μ," *Soviet Physics Uspekhi*, Vol. 10, No. 4, 509–514, 1968.
3. Khalaj-Amirhosseini, M., "Analysis of lossy inhomogeneous planar layers using the method of moments," *Journal of Electromagnetic Waves and Applications*, Vol. 21, 1925–1937, 2007.
4. Khalaj-Amirhosseini, M., "Analysis of lossy inhomogeneous planar layers using finite difference method," *Progress In Electromagnetics Research*, PIER 59, 187–198, 2006.

5. Rothwell, E. J., "Natural-mode representation for the field reflected by an inhomogeneous conductor-backed material layer — TE case," *Progress In Electromagnetics Research*, PIER 63, 1–20, 2006.
6. Kedar, A. and U. K. Revankar, "Parametric study of flat sandwich multilayer radome," *Progress In Electromagnetics Research*, PIER 66, 253–265, 2006.
7. Aissaoui, M., J. Zaghdoudi, M. Kanzari, and B. Rezig, "Optical properties of the quasi-periodic one-dimentional generalized multilayer Fibonacci structures," *Progress In Electromagnetics Research*, PIER 59, 69–83, 2006.
8. Qing, A. and C. K. Lee, "An improved model for full wave analysis of multilayered frequency selective surface with gridded square element," *Progress In Electromagnetics Research*, PIER 30, 285–303, 2001.
9. Kong, J. A., "Electromagnetic wave interaction with stratified negative isotropic media," *Progress In Electromagnetics Research*, PIER 35, 1–52, 2002.
10. Cory, H. and C. Zach, "Wave propagation in metamaterial multilayered structures," *Mic. and Opt. Tech. Lett.*, Vol. 40, No. 6, 460–465, 2004.
11. Oraizi, H. and M. Afsahi, "Analysis of planar dielectric multilayers as FSS by transmission line transfer matrix method (TLTMM)," *Progress In Electromagnetics Research*, PIER 74, 217–240, 2007.
12. Ishimaru, A., *Electromagnetic Wave Propagation, Radiation, and Scattering*, Englewood Cliffs, Prentice Hall, 1991.
13. Oraizi, H. and M. Afsahi, "Determination of correct values for propagation constant, intrinsic impedance and refraction index of metamaterials," *IEEE Int. Conf. Applied Electromagnetic*, 1–4, Kolkata, India, 2007.
14. Gerardin, J. and A. Lakhtakia, "Negative index of refraction and distributed Bragg reflectors," *Mic. and Opt. Tech. Lett.*, Vol. 34, No. 6, 409–411, 2002.
15. Zhang, Z. M. and C. J. Fu, "Unusual photon tunneling in the presence of a layer with a negative refractive index," *App. Phys. Lett.*, Vol. 80, No. 6, 1097–1099, 2002.
16. Gao, L. and C. J. Tang, "Near-field imaging by a multi-layer structure consisting of alternate right-handed and left-handed materials," *Phys. Lett. A*, Vol. 322, No. 5–6, 390–395, 2004.
17. Macleod, H. A., *Thin-Film Optical Filters*, 94–100, Adam Hilger, London, 1969.

18. de Gennes, P. G. and J. Prost, *The Physics of Liquid Crystals*, Sec. 6.1.2, Clarendon Press, Oxford, 1993.
19. Ghatak, A. and K. Thyagarajan, *Optical Electronics*, Cambridge University Press, Cambridge, 1989, Sec. 18.6.
20. Othonos, A., "Fiber Bragg ratings," *Rev. Sci. Instrum.*, Vol. 68, 4309–4341, 1997.
21. Pendry, J. B., "Negative refraction makes a perfect lens," *Phys. Rev. Lett.*, Vol. 85, No. 18, 3966–3969, 2000.
22. Oraizi, H. and M. Afsahi, "Lossless DNG-DPS bilayer structures for tunneling and zero reflection," *PIERS Online*, Vol. 4, No. 1, 69–72, 2008.
23. Ye, Z., "Optical transmission and reflection of perfect lenses by left handed materials," *Phys. Rev. B*, Vol. 67, No. 19, 193106: 1–4, 2003.
24. Garcia, M. and M. Nieto-Vesperinas, "Left-handed materials do not make a perfect lens," *Phys. Rev. Lett.*, Vol. 88, No. 20, 207403: 1–4, 2002.
25. Fu, C. and Z. M. Zhang, "Radiative properties of multilayer thin films with positive and negative refractive indexes," *ASME Int. Conf. Mechanical Engineering Congress & Exposition*, New Orleans, USA, 2002.
26. Besso, P., M. Bozzi, L. Perregrini, L. S. Drioli, and W. Nickerson, "Deep space antenna for Rosetta mission: Design and testing of the S/X-band dichroic mirror," *IEEE Trans. Antennas Propagat.*, Vol. 51, 388–394, 2003.
27. Pendry, J., A. Holden, and W. Stewart, "Magnetism from conductors and enhanced nonlinear phenomena," *IEEE Trans. Microwave Theory Tech.*, Vol. 47, No. 18, 2075–2084, 1999.
28. Smith, D. R., W. J. Padilla, D. C. Vier, S. C. Nemat-Nasser, and S. Schultz, "Composite medium with simultaneously negative permeability and permittivity," *Phys. Rev. Lett.*, Vol. 84, No. 18, 4184–4187, 2000.